Journal of Alloys and Compounds 835 (2020) 155347

Contents lists available at ScienceDirect

Journal of Alloys and Compounds

journal homepage: http://www.elsevier.com/locate/jalcom

Sintering-resistant platinum electrode achieved through atomic layer deposition for thin-film solid oxide fuel cells

Han Gil Seo [a, 1, 2], Sanghoon Ji [b, 1], Jongsu Seo [a], Sanwi Kim [c], Bonjae Koo [a, 3], Yoonseok Choi [a, 4], Hyunseung Kim [a], Jeong Hwan Kim [d], Taek-Soo Kim [c], WooChul Jung [a, *]

[a] Department of Materials Science and Engineering, Korea Advanced Institute of Science and Technology, 291 Daehak-ro, Yuseong-gu, Daejeon 34141, Republic of Korea
[b] Environmental Resource Research Center, Department of Land, Water and Environment Research, Korea Institute of Civil Engineering and Building Technology, 283 Goyang-daero, Ilsanseo-gu, Goyang 10223, Republic of Korea
[c] Department of Mechanical Engineering, Korea Advanced Institute of Science and Technology, 291 Daehak-ro, Yuseong-gu, Daejeon 34141, Republic of Korea
[d] Department of Advanced Materials Engineering, Hanbat National University, 125 Dongseo-daero, Yuseong-gu, Daejeon 34158, Republic of Korea

ARTICLE INFO

Article history:
Received 11 February 2020
Received in revised form
22 April 2020
Accepted 22 April 2020
Available online 28 April 2020

Keywords:
Thin-film solid oxide fuel cell
Atomic layer deposition
Al_2O_3
Pt electrode
Oxygen reduction reaction

ABSTRACT

Thin-film solid oxide fuel cells (TF-SOFCs) using a dense and thin electrolyte have attracted much attention as a promising portable power generator because they can lower the operating temperature of devices, which is a key issue related to conventional SOFCs, to below 500 °C and are compatible with several microfabrication processes. Highly porous interconnected Pt thin films are now widely used as oxygen electrodes, but their poor thermal stability seriously hampers the sustainable operation of TF-SOFCs. Here, we demonstrate how Al_2O_3 layers coated through atomic layer deposition effectively suppress the degradation of nanoporous Pt thin-film electrodes. Although Al_2O_3 is an electrical insulator, the selection of an appropriate overcoat thickness ensures stable electrochemical reaction sites of the Pt electrode at high temperatures even without serious current collection or gas flow issues. As a result, a 3.6-nm-thick Al_2O_3 layer maintains the high specific surface area morphology of Pt thin films at 450 °C and improves the electrode activity by more than twofold compared to an uncoated sample. These results suggest that a simple and scalable coating strategy enables the implementation of TF-SOFCs with ideal performance and durability outcomes.

1. Introduction

Solid oxide fuel cells (SOFCs) have attracted a considerable amount of attention as a promising electrochemical energy conversion device owing to their high conversion efficiency, fuel flexibility and low overall emissions [1]. However, the high temperature (>700 °C) required for their operation increases the material and system costs and shortens device lifetimes, which are grand challenges to those working toward SOFC commercialization [2–4]. Among the many attempts thus far to lower the operating temperature (<500 °C), thin-film-based SOFCs (TF-SOFCs) composed of a dense thin film of solid electrolyte between porous film electrodes have been actively studied in recent years [5–13]. The use of a thin electrolyte membrane can significantly reduce the ohmic resistance, even at reduced temperatures. Furthermore, TF-SOFCs can be miniaturized on Si or other commercially available wafers with microelectromechanical system (MEMS) components, making them easy to use in portable electronic devices. Nonetheless, the high electrochemical resistance of the essential cell components, the cathode in particular, at low temperatures remains the greatest obstacle preventing the implementation of high-

* Corresponding author.
E-mail address: wcjung@kaist.ac.kr (W. Jung).
[1] These authors contributed equally to this work.
[2] Current address: Department of Materials Science and Engineering, Massachusetts Institute of Technology, 77 Massachusetts Avenue, Cambridge, MA 02139, USA.
[3] Current address: Department of Mechanical Engineering, Massachusetts Institute of Technology, 77 Massachusetts Avenue, Cambridge, MA 02139, USA.
[4] Current address: Energy Materials Laboratory, Korea Institute of Energy Research, 152 Gajeong-ro, Yuseong-gu, Daejeon 34129, Republic of Korea.

https://doi.org/10.1016/j.jallcom.2020.155347
0925-8388/

performance TF-SOFCs [4,14,15].

In this regard, platinum (Pt) thin films are commonly used as a cathode material for TF-SOFCs due to the process compatibility of Pt with micro-fabrication techniques, its excellent electrochemical activity toward the oxygen reduction reaction (ORR), and its high electrical conductivity [16]. Furthermore, unlike other metals, Pt is very resistant to oxidation and is suitable for use in cathodes functioning in atmospheres containing oxygen gas [17,18]. For these reasons, despite the high cost of Pt, most high-performance TF-SOFCs reported thus far include Pt thin-film cathodes [8,13,19–22]. Because Pt has high reactivity to the adsorption and dissociation of oxygen molecules but low oxygen ion conductivity, the ORR reaction at the cathode mainly occurs at the triple-phase boundaries (TPBs), where the gas, electrolyte, and electrode come into contact [23,24]. Accordingly, in order to ensure the electrochemical performance of Pt electrodes deposited on solid oxide electrolytes such as yttria-stabilized zirconia (YSZ), the electrode must have a sufficiently long TPB length and an interconnected network architecture that enables electron and oxygen percolation pathways.

While various manufacturing tools such as electrospinning [25–27] and screen-printing [28,29] to fabricate porous electrode structures with a high density of reaction sites have been introduced thus far, sputtering is the simplest and most scalable means of manufacturing such a highly porous percolated Pt structure. By simply increasing the Ar deposition pressure (>50 mTorr) or feeding with O_2 reactive gas, a vertically oriented Pt thin film with a high TPB density level and specific surface area can be obtained without an additional template [30–34]. Meanwhile, previous efforts to utilize sputtered Pt thin films in TF-SOFCs are affected by the poor thermal stability of Pt. Nanostructured Pt films begin to sinter and agglomerate when they are heated to their required operating temperatures (typically 400–600 °C), and their electrochemical activity seriously degrades during long-term high-temperature operation [32,34–37]. Thus, it is essential to develop a technique that can maintain the nanoscale features of Pt thin films while improving their thermal stability at the same time.

Among the many efforts to solve these issues, a strategy of protecting Pt thin-film electrodes with thin oxide overcoats *via* atomic layer deposition (ALD) has attracted much attention [22,35,38,39]. ALD is a coating method capable of precise control of the thickness and uniformity of oxide overcoats. In addition, it has an additional advantage in that large-area deposition is possible without an additional high-temperature sintering process, making this process feasible for use to protect Pt electrode with a three-dimensional nanoporous structure. Recently, Shin et al. demonstrated the applicability of an ultrathin ceria (CeO_2) overlayer on the surfaces of porous Pt electrodes, improving the activation resistance by 50% and ensuring the thermal stability for 10 h at 450 °C [22]. Karimaghaloo et al. reported an enhanced power density of 5.6-fold with decent thermal stability for 14 h at 600 °C through the application of YSZ overcoats onto porous Pt electrodes [39].

Here, we report that a nanoscale Al_2O_3 overcoat on porous Pt films can effectively inhibit Pt agglomeration and greatly improve the electrode activity at 450 °C. Thin Al_2O_3 layers were synthesized on top of Pt with precise thickness control by means of ALD. The physical, chemical, and electrochemical properties of the Al_2O_3-decorated Pt electrodes were characterized by a range of analysis tools, in this case scanning electron microscopy (SEM), X-ray photoelectron spectroscopy (XPS), electrochemically active surface area (ECSA), AC impedance spectroscopy (ACIS), and double-cantilever-beam (DCB) stripping measurements. The self-limiting growth process of ALD makes it possible to deposit highly conformal Al_2O_3 films on vertically aligned columnar Pt structures and to form evenly distributed nanoscale Al_2O_3 clusters via a subsequent coarsening step under high-temperature operation. As a result, the isolated nanoclusters formed between the Pt columns prevent the sintering of the Pt while allowing the oxygen gas to reach the electrochemical reaction sites (Fig. 1). We observed that with an Al_2O_3 thickness of approximately 3.6 nm, the electrode activity is enhanced by more than double compared to a bare Pt thin-film electrode. This result is very surprising in that a complete insulator, Al_2O_3, covers the electrode surface, and we would like to emphasize that the unique ability of ALD to control the thickness to sub-nano levels in an extremely uniform manner gives the insulating material a new functionality. Despite previous reports that either ionic conducting oxides or metal catalysts were coated *via* ALD, sputtering, electrochemical deposition and infiltration on porous thin-film electrodes to improve the electrode performance [22,24,34,35,38–51], to the best of our knowledge, this is *the first report* of an improvement of the electrode performance and durability with Al_2O_3 ALD overcoats simultaneously.

2. Experimental

Highly porous Pt thin films with a thickness of 120 nm were fabricated on both sides of (100) single-crystal YSZ (8 mol%, 10 × 10 × 0.5 mm^3, MTI Corp.) substrates using the DC magnetron sputtering method. In the general physical vapor deposition method, the porosity of the deposited film is controlled by adjusting the pressure during the deposition process [52]. In this work, the sputtering system was operated at a DC power of 100 W in an Ar atmosphere with a working pressure of 60 mTorr.

An Al_2O_3 overcoat layer was deposited by ALD onto the Pt films for 30 and 50 cycles with trimethylaluminum ($Al_2(CH_3)_6$) as a precursor and diluted water as an oxidant at a substrate temperature of 233 °C. In a typical run, a number of Pt/YSZ/Pt symmetrical cells were placed on a custom-made metal holder in the middle of the reactor. A typical coating cycle used the following sequence: Al precursor dose (0.5 s) – Ar purge (5 s) – water dose (1 s) – Ar purge (15 s). The self-limiting growth behavior of the ALD process is shown in Fig. S1. The Al_2O_3 layers were deposited at a constant growth rate regardless of the precursor pursing time (more than 0.5 s), indicative of uniform layer-by-layer growth. The growth rate (1.2 Å/cycle) of the Al_2O_3 layers was determined and used to calculate the precise thickness of the Al_2O_3 overcoats corresponding to 30 and 50 cycles. The resulting thicknesses after 30 and 50 cycles were determined to 3.6 nm and 6.0 nm, respectively.

Delamination of the Pt layer from YSZ substrate was achieved using the double-cantilever-beam (DCB) test method. The DCB technique is a popular fracture mechanic testing method which applies a load during delamination only in the direction normal to the crack plane (Mode I loading). Because there is no shear movement of the Pt layer, the original interface morphology between Pt and YSZ can be preserved. This method has been applied previously to achieve true TPBs of porous Pt layers [32]. In this study, all of the porous Pt thin films deposited onto the YSZ substrates (with or without Al_2O_3 layer) were cleaved into 10 × 30 mm^2 to constitute the DCB delamination samples. A dummy silicon substrate was also prepared at the same size described above and coated with an epoxy adhesive (Epo-Tek 353ND; Epoxy Technology, USA). The porous Pt/YSZ substrate was then bonded with the dummy silicon substrate and cured at 120 °C for 2 h to create a the Si/epoxy/Pt bond. Finally, the bonded DCB specimen was mounted on a high-precision micromechanical test system (Delaminator Adhesion Test System, DTS Company, USA) for delamination by the DCB test method.

The microstructures of both bare and Al_2O_3-coated Pt films were examined by means of scanning electron microscopy (SEM, Hitachi S-4800). After DCB delamination, the porosity and TPB density

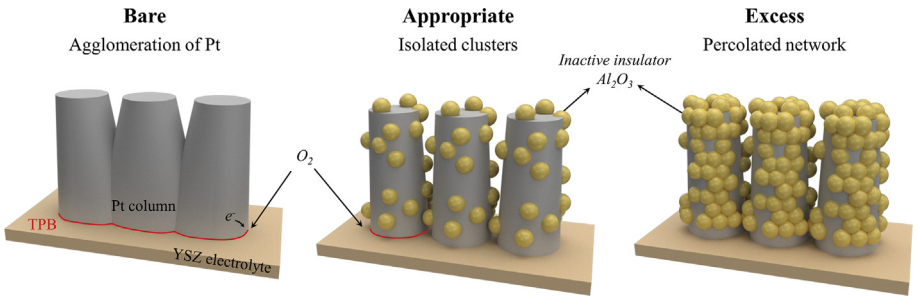

Fig. 1. Schematic comparison of the morphological evolution between bare and Al_2O_3-coated Pt thin films with respect to the number of atomic layer deposition (ALD) cycles.

levels of both films at the Pt/YSZ interfaces were estimated by an image analysis using ImageJ software (U.S. National Institutes of Health, 1.48v).

The electrochemical characteristics of symmetric cells with identically sized (10 × 10 mm^2) bare and Al_2O_3-coated Pt electrodes were measured by AC impedance spectroscopy (ACIS, VSP-300, Biologic). AC amplitude of 20 mV at a frequency range of 2 MHz–4 mHz was used. ACIS was carried out at temperatures between 400 and 500 °C at an oxygen partial pressure of 0.21 atm.

Cyclic voltammetry (CV) was performed in a standard three-electrode system composed of the Pt thin film as the working electrode (held in a place using aluminum clips), a counter electrode (Pt wire, Alfa Aesar) and a reference electrode (saturated calomel electrode (SCE, +0.255 V vs. standard hydrogen electrode (SHE)), Koslow). After annealing at 450 °C for 10 h, each electrode was immersed in a 0.5 M H_2SO_4 solution with a constant distance relative to the other electrodes and with a constant depth in the solution. Ten consecutive CVs were measured in the potential range of −0.255 to 1.255 V vs. SCE with a scan rate of 50 mV s^{-1}. The ECSA of the Pt thin film calculated upon the monolayer adsorption of hydrogen is equal to 210 μC cm^{-2}. The specific surface area was determined from the ratio of ECSA to the Pt loading thickness.

X-ray photoelectron spectroscopy (XPS, K-alpha, Thermo VG Scientific) of the surface of the Pt/YSZ interface after delamination of the 30-cycle Al_2O_3-coated Pt electrode was conducted under an ultrahigh vacuum using Al Kα (hν = 1486.6 eV) radiation with a monochromatic beam with a diameter of 30 μm. All binding energy outcomes from the XPS spectra were referenced to the C 1s peak at 284.8 eV, as shown in Fig. S2.

3. Results and discussion

Fig. 2 shows SEM images (top view) of both bare and Al_2O_3-coated Pt films with respect to the ALD cycles. Highly porous Pt thin films with a thickness of 120 nm were fabricated by sputtering at a high Ar pressure (>50 mTorr). The Pt grows in the form of vertically aligned columns each with a diameter of about 20 nm. The as-deposited Pt thin films exhibited several or tens of nanometers of pores between vertical Pt columns, giving oxygen gas molecules easy access to the TPBs. As the number of ALD cycles increases, the Al_2O_3 coating layer thickens and the nanoscale pores disappear, eventually leaving the entire surface of each Pt column covered with Al_2O_3 (Fig. 2(c) and (e)). For example, with 30 cycles of ALD (~3.6 nm in thickness), the shape of the thin film does not differ greatly from that of bare Pt, forming isolated clusters with almost no charging effect caused by the Al_2O_3 coating. In contrast, thick Al_2O_3 overcoats of approximately 6 nm deposited by 50 cycles have the structure of a percolated network, as shown in Fig. 1, with a severe charging effect, compared to the bare and 30-cycle cases, consistent with a previous study of ALD ZrO_2 on dense Pt thin films [38]. Thus, the layer nearly covers all of the nanoscale pores and hinders the supply of oxygen gas. Because Al_2O_3 is an inactive insulator, such thick overcoats are expected to block the flow of electronic current as well as the supply of oxygen, resulting in a significant reduction in the ORR performance. Fig. 2 (b), (d), and (f) show how the surface morphology of each sample changed according to an ACIS analysis (at 400–500 °C, for 10 h). The bare Pt electrode shows that the vertical grown nano-columns are heavily agglomerated, whereas the Al_2O_3-coated samples are much less sintered. Moreover, the thicker the Al_2O_3 overcoat is, the better the sintering resistance between the Pt columns becomes. Therefore, it can be concluded that the Al_2O_3 coating strategy has the beneficial effect of stabilizing these nanoporous Pt structures according to top-view microstructural observations of the Pt electrode.

Next, the electrochemical performance of the Al_2O_3-coated porous Pt films was investigated by ACIS with respect to the number of ALD cycles at temperatures between 400 °C and 500 °C in air. The complex impedance spectra for symmetric Pt|YSZ|Pt cells with or without an Al_2O_3 overcoat, plotted in Nyquist form, commonly consist of two adjacent semicircles, which are distinguished as a nearly ideal high-frequency (HF) and a slightly distorted low-frequency (LF) semicircle, respectively (Fig. 3). The impedance spectra were well modeled by a series of two parallel *RQ* sub-circuits, as shown in the inset, where *R* is the resistance, *Q* is the constant-phase element (CPE), the overall impedance is

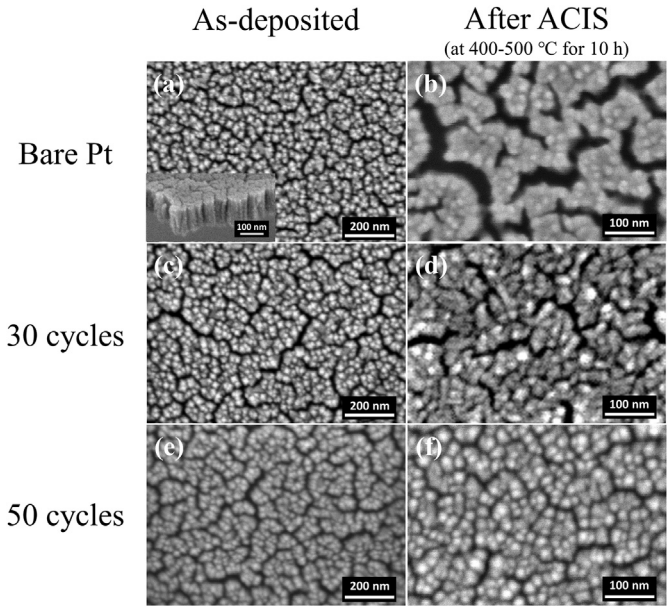

Fig. 2. Top-view SEM images of bare and Al_2O_3-coated Pt electrodes before and after ACIS measurements at temperatures of 400–500 °C for 10 h: (a, b) bare, (c, d) 30-cycle, and (e, f) 50-cycle Al_2O_3-coated Pt electrodes.

determined by $Z_Q = 1/Q(i\omega)^n$, n is a constant, and ω is the frequency. The capacitance of this response was calculated according to $C = (R^{1-n}Q)^{1/n}$ [53]. This equation is generally used with Pt electrodes on YSZ electrolytes in the literature [33,34,54]. Given the conductivity and dielectric constant of YSZ and the cell dimensions used in this study, the HF impedance spectra are readily attributed to the YSZ electrolyte [55,56]. Thus, the LF impedance reflects the characteristics of the ORR at the Pt thin-film electrodes. This is also supported by the fact that the LF arcs of all samples have large capacitance values (4 - 7 × 10^{-5} Fcm^{-2}), which are well known to be associated with the double-layer capacitance of typical Pt thin films on YSZ [33,57]. The resistance of the electrode is changed considerably by the addition of the Al_2O_3 overcoat. Interestingly, a Pt electrode coated with 30 cycles of Al_2O_3 via ALD showed lower electrode resistance by more than twofold at 450 °C in air as compared to the outcome with bare Pt, whereas ALD at 50 cycles substantially increases the electrode resistance. For example, the electrode conductance outcomes for 30 cycles and 50 cycles of Al_2O_3 ALD are 1.4 × 10^{-3} Scm^{-2} and 2.9 × 10^{-4} Scm^{-2}, respectively, compared to that of bare Pt (6.2 × 10^{-4} Scm^{-2}). Arrhenius plots of the electrode resistance levels of bare and 30-cycle Al_2O_3-coated Pt measured at $P_{O_2} = 0.21$ atm are presented in Fig. S3, demonstrating the activation energy (E_a) associated with the ORR; the corresponding E_a values of the bare and 30-cycle Al_2O_3-coated Pt electrodes are 1.31 and 1.35 eV, respectively, close to that of Pt thin-film electrodes in the literature [33,34,58]. Regardless of the Al_2O_3 overcoat, a constant value of E_a indicates no change in the ORR mechanism, confirming that Al_2O_3 does not function as an ORR catalyst. While the detailed ORR mechanism is not covered in this work, the measured E_a values of both electrodes may represent a clue regarding the ORR mechanism. According to the literature on the ORR of Pt electrodes at low temperatures (<500 °C), oxygen diffusion on the Pt surface to TPBs can be a key step in determining the overall rate of the ORR process with E_a values between 1.1 and 1.3 eV, consistent with our findings [59,60]. This can be interpreted as meaning that 30 cycles of Al_2O_3 ALD resulted in isolated nanoclusters that did not affect the surface diffusion rate of oxygen species, allowing the maintenance of high TPB densities by physically preventing the sintering of Pt. Excessive Al_2O_3 overcoat layers, however, may form a percolated Al_2O_3 network which likely impedes the surface diffusion of oxygen species to the TPB.

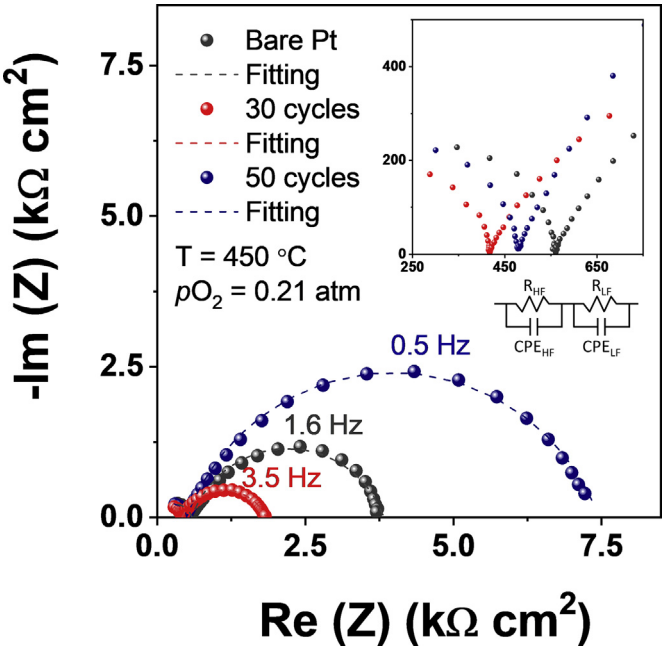

Fig. 3. Typical impedance spectra of bare and Al_2O_3-coated Pt electrodes with respect to the number of ALD cycles measured at 450 °C with $P_{O_2} = 0.21$ atm.

Earlier studies reported an enhancement of the performance and stability of porous thin-film metal (i.e., Pt and Ag) electrodes with the use of ALD overcoats [22,35,38–40,48]. For example, Shin et al. recently attempted to coat the surface of Pt with an ultrathin ceria (CeO_2) overlayer; the resulting films enhanced the peak power density by 30% and exhibited thermal stability for 10 h compared to an uncoated sample [22]. Liu et al. reported improved ORR activity and stability of Pt cathodes with ALD-zirconia (ZrO_2) overcoats at a temperature of 450 °C [38]. Chang et al. fabricated YSZ-coated Pt thin-film electrodes, showing an enhancement of the power density by 2.5 times and good stability at 500 °C [35]. The studies above focused on the use of a zirconia- or ceria-based overcoats because these materials can also function as an ORR catalyst, such as for oxygen adsorption [61,62], and/or can provide oxygen ionic pathways to enhance TPB sites during the device operation [63,64]. Considering the ALD coating materials in earlier studies, our observation is surprising given that Al_2O_3 is a dielectric. As will be discussed later, it is interpreted that the improved electrode reactivity, even when the surface of the Pt electrode is partially covered with an insulator, stems from the Al_2O_3 overcoat, which more effectively inhibits the deterioration of the Pt electrode driven by sintering. Notably, the fine thickness difference in the Al_2O_3 overcoats (3.6 nm and 6.0 nm, respectively for 30 and 50 cycles) causes the Pt electrode ORR to vary by a factor of five, demonstrating the significance of the capability of the ALD process to control the thickness and coverage at the sub-nanoscale level for our strategy. In addition, the thermal stability levels of both the bare and 30-cycle Al_2O_3-coated Pt thin-film electrodes were evaluated at a relatively high temperature of 550 °C for 10 h (Fig. S4) to accelerate the sintering of Pt thin films. It was found that the 30-cycle Al_2O_3-coated Pt electrode exhibited greatly improved the thermal stability compared to the bare Pt electrode, demonstrating again that the Al_2O_3 overcoat extends the durability of the Pt electrode.

To verify the role of the nanoscale Al_2O_3 overcoats on the electrode performance and durability, we analyzed the structure and composition near the Pt interface connected to the YSZ electrolyte by the DCB stripping technique (Fig. 4(a)). This method was introduced by Yu et al., in 2015, and they directly observed thermally driven morphological evolution between the top surfaces of porous Pt electrodes and Pt/YSZ interfaces [32]. They also reported that nanoscale pores of Pt/YSZ interfaces have better thermal stability than Pt surfaces. In this regard, it must be important directly to identify the changes in the TPB density levels where the actual ORR occurs at Pt/YSZ interfaces during device operation, as opposed to TPBs estimated from Pt top surfaces. After DCB delamination, interfacial SEM micrographs of bare Pt and 30-cycle Al_2O_3-coated Pt film samples annealed at 450 °C for 10 h are shown in Fig. 4(b) and (c), respectively. The 30-cycle Al_2O_3 layer shows that the Pt thin films maintain a sufficient level of porosity with nanoscale pores at 450 °C, allowing oxygen gas molecules ready access to the TPB, with the corresponding TPB density being several tens of nanometers or less. The porosity and TPB density values of both the bare and 30-cycle Al_2O_3-coated Pt thin films as determined from an SEM image analysis are summarized in Table 1. This can confirm that the Al_2O_3 ALD layer retains a porosity rate of 30% and TPB density of 202 $\mu m \cdot \mu m^{-2}$, exceeding those of bare Pt (23%, 88 $\mu m \cdot \mu m^{-2}$). The Pt interfacial region near YSZ is a key active site where the ORR takes place. Therefore, it is evident that the reduction of the electrode resistance by half due to the Al_2O_3 overcoat stems from the TPB density, which increased from 88 $\mu m \cdot \mu m^{-2}$ to 202 $\mu m \cdot \mu m^{-2}$,

approximately doubling. This is further supported by the ECSA results showing the exposed electrochemically active Pt surface area. Even after annealing at 450 °C for 10 h, the calculated specific ECSA of the 30-cycle Al_2O_3-coated Pt electrode, 5.7 m^2/g_{Pt}, is approximately 40% higher than that of the bare Pt electrode (4.1 m^2/g_{Pt}) (Table 1 and Fig. S5).

Apart from the geometrical effect of Pt thin films, it is necessary to confirm whether the inactive insulator Al_2O_3 penetrates the electrode through nanopores to the YSZ electrolyte and blocks ORR active sites near the TPBs. For this purpose, with delaminated 30-cycle Al_2O_3-coated thin films, we also carried out an XPS analysis to confirm whether or not Al species exist near the TPB area (Fig. 4(d)–(e)). The binding energy peak positioned at 118 eV corresponding to Al 2s was used [65], and it was clearly found that no detectable intensity of Al existed even after the ALD process and subsequent annealing at 450 °C for 10 h. Therefore, it can be concluded that Al_2O_3 overcoats are selectively present only between the Pt columns and not at the TPBs, thereby preventing Pt sintering without affecting the chemistry of the Pt/YSZ interfaces in the operating environment.

4. Conclusions

We designed and fabricated Al_2O_3-decorated Pt thin-film electrodes through ALD with precise thickness control in an effort to inhibit Pt agglomeration and improve the ORR activity simultaneously. Interestingly, 30 cycles (3.6 nm in thickness) of deposition of the inactive insulator Al_2O_3 have direct effects on the electrode performance, ECSA and TPB densities, which were derived as follows:

- The Al_2O_3 overcoats improve the electrode performance of Pt thin films by more than twofold.

Table 1
The porosity, TPB density and ECSA of bare and 30-cycle Al_2O_3-coated Pt electrodes after a heat treatment at 450 °C for 10 h.

Al_2O_3 ALD cycle	Porosity (%)	TPB length ($\mu m \cdot \mu m^{-2}$)	ECSA (m^2/g_{Pt})
0	23[a]	88[a]	4.1
30	32[a]	202[a]	5.7

[a] Pt-YSZ interfaces after DCB delamination.

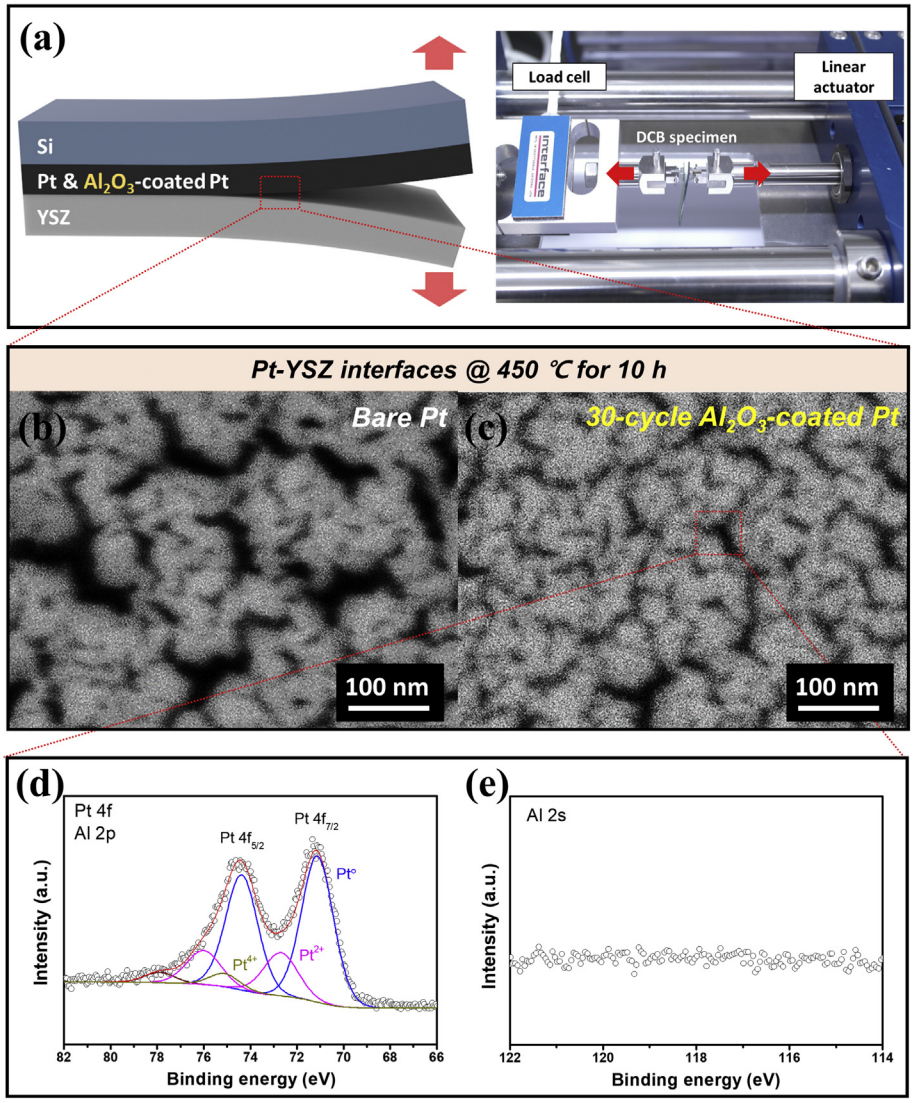

Fig. 4. (a) Schematic and photograph of the DCB stripping method. SEM images of (b) bare and (c) 30-cycle Al_2O_3-coated Pt electrodes at Pt/YSZ interfaces after annealing at 450 °C for 10 h, (d, e) XPS results of 30-cycle Al_2O_3-coated Pt electrodes with (d) Pt 4f and (e) Al 2s spectra.

- ECSA of the Al_2O_3-coated Pt electrode exhibits a 40% higher value of 5.7 m^2/g_{Pt} compared to that of an uncoated Pt electrode (4.1 m^2/g_{Pt}).
- The isolated Al_2O_3 clusters maintain the TPB densities (202 $\mu m \cdot \mu m^{-2}$) at a level of more than twice that of an uncoated Pt electrode (88 $\mu m \cdot \mu m^{-2}$).

Further, to verify the role of the Al_2O_3 overcoat on the thermal stability and electrochemical performance, we initially confirmed that there is no Al_2O_3 at the Pt/YSZ interfaces, indicating that the incorporation of oxygen species into the electrolyte lattice is unimpeded. Second, we found that the initial Al_2O_3 layer takes on a scattered cluster form at the required operating temperatures, thereby acting as a sintering resistor which simply prevents Pt sintering without interfering with the oxygen gas adsorption/dissociation process or the diffusion of oxygen species onto the Pt surface. To the best of our knowledge, no attempt has been made to confirm the presence or absence of an ALD oxide coating layer by a combination of delamination and an XPS analysis despite the numerous studies of ALD oxide coatings for TF-SOFCs. The findings here thus provide a guideline for improving the thermal stability against sintering and improving the electrode activity with the use of an ultra-thin oxide layer.

Author contributions

H.G. Seo, S. Ji and W. Jung conceived of and designed the project. J. Seo, H. Kim and J.H. Kim conducted the sample preparation. S. Kim and T.-S. Kim performed the DCB striping measurements. B. Koo and Y. Choi undertook the XPS analysis and ECSA experiments. All authors participated in discussions of the results and assisted in writing the manuscript.

Declaration of competing interest

The authors declare that they have no known competing financial interests or personal relationships that could have appeared to influence the work reported in this paper.

CRediT authorship contribution statement

Han Gil Seo: Conceptualization, Investigation, Writing - original draft. **Sanghoon Ji:** Conceptualization, Investigation, Writing - review & editing. **Jongsu Seo:** Investigation. **Sanwi Kim:** Investigation. **Bonjae Koo:** Investigation. **Yoonseok Choi:** Investigation. **Hyunseung Kim:** Investigation. **Jeong Hwan Kim:** Resources, Writing - review & editing. **Taek-Soo Kim:** Resources, Writing - review & editing. **WooChul Jung:** Supervision.

Acknowledgements

This work was supported by the Korea Institute of Energy Technology Evaluation and Planning (KETEP) and the Ministry of Trade, Industry and Energy (MOTIE) of the Republic of Korea (No. 20173020032120).

Appendix A. Supplementary data

Supplementary data to this article can be found online at https://doi.org/10.1016/j.jallcom.2020.155347.

References

[1] N.Q. Minh, Ceramic fuel-cells, J. Am. Ceram. Soc. 76 (1993) 563–588.
[2] E.D. Wachsman, K.T. Lee, Lowering the temperature of solid oxide fuel cells, Science 334 (2011) 935–939.
[3] H.L. Tuller, S.J. Litzelman, W. Jung, Micro-ionics: next generation power sources, Phys. Chem. Chem. Phys. 11 (2009) 3023–3034.
[4] N.P. Brandon, S. Skinner, B.C.H. Steele, Recent advances in materials for fuel cells, Annu. Rev. Mater. Res. 33 (2003) 183–213.
[5] J. An, J.H. Shim, Y.B. Kim, J.S. Park, W. Lee, T.M. Gur, F.B. Prinz, MEMS-based thin-film solid-oxide fuel cells, MRS Bull. 39 (2014) 798–804.
[6] D. Beckel, A. Bieberle-Hutter, A. Harvey, A. Infortuna, U.P. Muecke, M. Prestat, J.L.M. Rupp, L.J. Gauckler, Thin films for micro solid oxide fuel cells, J. Power Sources 173 (2007) 325–345.
[7] S. Ji, H.G. Seo, S. Lee, J. Seo, Y. Iee, W.H. Tanveer, S.W. Cha, W. Jung, Integrated design of a Ni thin-film electrode on a porous alumina template for affordable and high-performance low-temperature solid oxide fuel cells, RSC Adv. 7 (2017) 23600–23606.
[8] C.W. Kwon, J.W. Son, J.H. Lee, H.M. Kim, H.W. Lee, K.B. Kim, High-performance micro-solid oxide fuel cells fabricated on nanoporous anodic aluminum oxide templates, Adv. Funct. Mater. 21 (2011) 1154–1159.
[9] C.W. Kwon, J.I. Lee, K.B. Kim, H.W. Lee, J.H. Lee, J.W. Son, The thermo-mechanical stability of micro-solid oxide fuel cells fabricated on anodized aluminum oxide membranes, J. Power Sources 210 (2012) 178–183.
[10] Y.H. Lee, H. Ren, E.A. Wu, E.E. Fullerton, Y.S. Meng, N.Q. Minh, All-sputtered, superior power density thin-film solid oxide fuel cells with a novel nano-fibrous ceramic cathode, Nano Lett. (2020), https://doi.org/10.1021/acs.nanolett.9b02344.
[11] G.Y. Cho, Y.H. Lee, W. Yu, J. An, S.W. Cha, Optimization of Y_2O_3 dopant concentration of yttria stabilized zirconia thin film electrolyte prepared by plasma enhanced atomic layer deposition for high performance thin film solid oxide fuel cells, Energy 173 (2019) 436–442.
[12] S. Lee, Y. Lee, J. Park, W. Yu, G.Y. Cho, Y. Kim, S.W. Cha, Effect of plasma-enhanced atomic layer deposited YSZ inter-layer on cathode interface of GDC electrolyte in thin film solid oxide fuel cells, Renew. Energy 144 (2019) 123–128.
[13] S. Oh, J. Park, J.W. Shin, B.C. Yang, J.M. Zhang, D.Y. Jang, J. An, High performance low-temperature solid oxide fuel cells with atomic layer deposited-yttria stabilized zirconia embedded thin film electrolyte, J. Mater. Chem. A 6 (2018) 7401–7408.
[14] S.B. Adler, Factors governing oxygen reduction in solid oxide fuel cell cathodes, Chem. Rev. 104 (2004) 4791–4843.
[15] V. Metlenko, W. Jung, S.R. Bishop, H.L. Tuller, R.A. De Souza, Oxygen diffusion and surface exchange in the mixed conducting oxides $SrTi_{1-y}Fe_yO_{3-d}$, Phys. Chem. Chem. Phys. 18 (2016) 29495–29505.
[16] Y. Nie, L. Li, Z.D. Wei, Recent advancements in Pt and Pt-free catalysts for oxygen reduction reaction, Chem. Soc. Rev. 44 (2015) 2168–2201.
[17] Y. Abe, M. Kawamura, K. Sasaki, Effects of oxygen gettering and target mode change in the formation process of reactively sputtered Pt oxide thin films, J. Vac. Sci. Technol., A 18 (2000) 2608–2612.
[18] Y. Abe, M. Kawamura, K. Sasaki, Preparation of PtO and α-PtO_2 thin films by reactive sputtering and their electrical properties, Jpn. J. Appl. Phys. 38 (1999) 2092–2096.
[19] C.C. Chao, C.M. Hsu, Y. Cui, F.B. Prinz, Improved solid oxide fuel cell performance with nanostructured electrolytes, ACS Nano 5 (2011) 5692–5696.
[20] P.C. Su, C.C. Chao, J.H. Shim, R. Fasching, F.B. Prinz, Solid oxide fuel cell with corrugated thin film electrolyte, Nano Lett. 8 (2008) 2289–2292.
[21] K. Kerman, B.K. Lai, S. Ramanathan, Pt/$Y_{0.16}Zr_{0.84}O_{1.92}$/Pt thin film solid oxide fuel cells: electrode microstructure and stability considerations, J. Power Sources 196 (2011) 2608–2614.
[22] J.W. Shin, S. Oh, S. Lee, J.G. Yu, J. Park, D. Go, B.C. Yang, H.J. Kim, J. An, Ultrathin atomic layer-deposited CeO_2 overlayer for high-performance fuel cell electrodes, ACS Appl. Mater. Interfaces 11 (2019) 46651–46657.
[23] T. Ryll, H. Galinski, L. Schlagenhauf, P. Elser, J.L.M. Rupp, A. Bieberle-Hutter, L.J. Gauckler, Microscopic and nanoscopic three-phase-boundaries of platinum thin-film electrodes on YSZ electrolyte, Adv. Funct. Mater. 21 (2011) 565–572.
[24] H.G. Seo, Y. Choi, W. Jung, Exceptionally enhanced electrode activity of (Pr,Ce)$O_{2-\delta}$-Based cathodes for thin-film solid oxide fuel cells, Adv. Energy Mater. 8 (2018) 1703647.
[25] J. Parbey, M. Xu, J.L. Lei, M. Espinoza-Andaluz, T.S. Li, M. Andersson, Electrospun fabrication of nanofibers as high-performance cathodes of solid oxide fuel cells, Ceram. Int. 46 (2020) 6969–6972.
[26] T. Larsson, T.S. Li, M. Xu, I. Fransson, G.S. Yu, M. Andersson, B.H. Li, B. Sunden, Co-fabrication of nickel-YSZ cermet nanofibers via an electrospinning technique, Mater. Res. Bull. 86 (2017) 38–43.
[27] Y. Chen, Y.F. Bu, B.T. Zhao, Y.X. Zhang, D. Ding, R.Z. Hu, T. Wei, B. Rainwater, Y. Ding, F.L. Chen, C.H. Yang, J. Liu, M.L. Liu, A durable, high-performance hollow-nanofiber cathode for intermediate-temperature fuel cells, Nano Energy 26 (2016) 90–99.
[28] J.B. Liu, A.C. Co, S. Paulson, V.I. Birss, Oxygen reduction at sol-gel derived $La_{0.8}Sr_{0.2}Co_{0.8}Fe_{0.2}O_3$ cathodes, Solid State Ionics 177 (2006) 377–387.
[29] Y.J. Leng, S.H. Chan, K.A. Khor, S.P. Jiang, Performance evaluation of anode-supported solid oxide fuel cells with thin film YSZ electrolyte, Int. J. Hydrogen Energy 29 (2004) 1025–1033.
[30] H. Huang, M. Nakamura, P.C. Su, R. Fasching, Y. Saito, F.B. Prinz, High-performance ultrathin solid oxide fuel cells for low-temperature operation, J. Electrochem. Soc. 154 (2007) B20–B24.
[31] K. Kerman, B.K. Lai, S. Ramanathan, Nanoscale compositionally graded thin-

film electrolyte membranes for low-temperature solid oxide fuel cells, Adv. Energy Mater. 2 (2012) 656–661.
[32] C.C. Yu, S. Kim, J.D. Baek, Y. Li, P.C. Su, T.S. Kim, Direct observation of nanoscale Pt electrode agglomeration at the triple phase boundary, ACS Appl. Mater. Interfaces 7 (2015) 6036–6040.
[33] W. Jung, J.J. Kim, H.L. Tuller, Investigation of nanoporous platinum thin films fabricated by reactive sputtering: application as micro-SOFC electrode, J. Power Sources 275 (2015) 860–865.
[34] H.G. Seo, Y. Choi, B. Koo, A. Jang, W. Jung, Robust nano-architectured composite thin films for a low-temperature solid oxide fuel cell cathode, J. Mater. Chem. A 4 (2016) 9394–9402.
[35] I. Chang, S. Ji, J. Park, M.H. Lee, S.W. Cha, Ultrathin YSZ coating on Pt cathode for high thermal stability and enhanced oxygen reduction reaction activity, Adv. Energy Mater. 5 (2015) 1402251.
[36] X.H. Wang, H. Huang, T. Holme, X. Tian, F.B. Prinz, Thermal stabilities of nanoporous metallic electrodes at elevated temperatures, J. Power Sources 175 (2008) 75–81.
[37] B.K. Park, H.G. Seo, W. Jung, J.W. Lee, Perovskite oxide-based nanohybrid for low-temperature thin-film solid oxide fuel cells fabricated via a facile and scalable electrochemical process, Ceram. Int. 44 (2018) 18727–18735.
[38] K.Y. Liu, L.D. Fan, C.C. Yu, P.C. Su, Thermal stability and performance enhancement of nano-porous platinum cathode in solid oxide fuel cells by nanoscale ZrO_2 capping, Electrochem. Commun. 56 (2015) 65–69.
[39] A. Karimaghaloo, A.M. Andrade, S. Grewal, J.H. Shim, M.H. Lee, Mechanism of cathodic performance enhancement by a few-nanometer- thick oxide overcoat on porous Pt cathodes of solid oxide fuel cells, ACS Omega 2 (2017) 806–813.
[40] Y.K. Li, H.J. Choi, H.K. Kim, N.K. Chean, M. Kim, J. Koo, H.J. Jeong, D.Y. Jang, J.H. Shim, Nanoporous silver cathodes surface-treated by atomic layer deposition of Y:ZrO_2 for high-performance low-temperature solid oxide fuel cells, J. Power Sources 295 (2015) 175–181.
[41] H.J. Jeong, J.W. Kim, K. Bae, H. Jung, J.H. Shim, Platinum–Ruthenium heterogeneous catalytic anodes prepared by atomic layer deposition for use in direct methanol solid oxide fuel cells, ACS Catal. 5 (2015) 1914–1921.
[42] H.J. Jeong, J.W. Kim, D.Y. Jang, J.H. Shim, Atomic layer deposition of ruthenium surface-coating on porous platinum catalysts for high-performance direct ethanol solid oxide fuel cells, J. Power Sources 291 (2015) 239–245.
[43] J.H. Shim, G.D. Han, H.J. Choi, Y. Kim, S.C. Xu, J. An, Y.B. Kim, T. Graf, T.D. Schladt, T.M. Gur, F.B. Prinz, Atomic layer deposition for surface engineering of solid oxide fuel cell electrodes, International Journal of Precision Engineering and Manufacturing-Green Technology 6 (2019) 629–646.
[44] J.W. Shin, D. Go, S.H. Kye, S. Lee, J. An, Review on process-microstructure-performance relationship in ALD-engineered SOFCs, J. Phys.: Energy 1 (2019), 042002.
[45] H.J. Jeong, J.W. Kim, K. Bae, H. Jung, J.H. Shim, Platinum-Ruthenium heterogeneous catalytic anodes prepared by atomic layer deposition for use in direct methanol solid oxide fuel cells, ACS Catal. 5 (2015) 1914–1921.
[46] D.H. Kim, K. Bae, H.J. Choi, J.H. Shim, Ag surface-coated with nano-YSZ as an alternative to Pt catalyst for low-temperature solid oxide fuel cells, J. Alloys Compd. 769 (2018) 545–551.
[47] H.J. Choi, M. Kim, K.C. Neoh, D.Y. Jang, H.J. Kim, J.M. Shin, G.-T. Kim, J.H. Shim, High-performance silver cathode surface treated with scandia-stabilized zirconia nanoparticles for intermediate temperature solid oxide fuel cells, Adv. Energy Mater. 7 (2017) 1601956.
[48] K.C. Neoh, G.D. Han, M. Kim, J.W. Kim, H.J. Choi, S.W. Park, J.H. Shim, Nanoporous silver cathode surface treated by atomic layer deposition of CeO_x for low-temperature solid oxide fuel cells, Nanotechnology 27 (2016) 185403.
[49] Y. Choi, J. Kim, H.G. Seo, H.L. Tuller, W. Jung, Nucleation and growth kinetics of electrochemically deposited ceria nanostructures for high-temperature electrocatalysis, Electrochim. Acta 316 (2019) 273–282.
[50] Y. Choi, E.C. Brown, S.M. Haile, W. Jung, Electrochemically modified, robust solid oxide fuel cell anode for direct-hydrocarbon utilization, Nano Energy 23 (2016) 161–171.
[51] A. Buyukaksoy, V. Petrovsky, F. Dogan, Solid oxide fuel cells with symmetrical Pt-YSZ electrodes prepared by YSZ infiltration, J. Electrochem. Soc. 160 (2013) F482–F486.
[52] T.-S. Oh, Y.S. Tokpanov, Y. Hao, W. Jung, S.M. Haile, Determination of optical and microstructural parameters of ceria films, J. Appl. Phys. 112 (2012) 103535.
[53] J. Pena-Martinez, D. Marrero-Lopez, J.C. Ruiz-Morales, P. Nunez, C. Sanchez-Bautista, A.J. Dos Santos-Garcia, J. Canales-Vazquez, On $Ba_{0.5}Sr_{0.5}Co_{1-y}Fe_yO_{3-\delta}$ (y=0.1-0.9) oxides as cathode materials for $La_{0.9}Sr_{0.1}Ga_{0.8}Mg_{0.2}O_{2.85}$ based IT-SOFCs, Int. J. Hydrogen Energy 34 (2009) 9486–9495.
[54] J.L. Hertz, A. Rothschild, H.L. Tuller, Highly enhanced electrochemical performance of silicon-free platinum–yttria stabilized zirconia interfaces, J. Electroceram. 22 (2008) 428–435.
[55] W.D. Shen, J.L. Hertz, Ionic conductivity of YSZ/CZO multilayers with variable lattice mismatch, J. Mater. Chem. A 3 (2015) 2378–2386.
[56] M.C. Steil, F. Thevenot, M. Kleitz, Densification of yttria-stabilized zirconia - impedance spectroscopy analysis, J. Electrochem. Soc. 144 (1997) 390–398.
[57] N.L. Robertson, J.N. Michaels, Double layer capacitance of porous platinum electrodes in zirconia electrochemical cells, J. Electrochem. Soc. 138 (1991) 1494–1499.
[58] A.K. Opitz, J. Fleig, Investigation of O_2 reduction on Pt/YSZ by means of thin film microelectrodes: the geometry dependence of the electrode impedance, Solid State Ionics 181 (2010) 684–693.
[59] D.Y. Wang, Low-temperature diffusion-controlled polarization of Pt electrodes with yttria-stabilized zirconia electrolyte, J. Electrochem. Soc. 137 (1990) 3660–3666.
[60] D.Y. Wang, A.S. Nowick, Diffusion-controlled polarization of Pt, Ag, and Au electrodes with doped ceria electrolyte, J. Electrochem. Soc. 128 (1981) 55–63.
[61] X. Xia, R.J. Oldman, C.R.A. Catlow, Oxygen adsorption and dissociation on yttria stabilized zirconia surfaces, J. Mater. Chem. 22 (2012) 8594–8612.
[62] Z.L. Wu, M.J. Li, J. Howe, H.M. Meyer, S.H. Overbury, Probing defect sites on CeO_2 nanocrystals with well-defined surface planes by Raman spectroscopy and O_2 adsorption, Langmuir 26 (2010) 16595–16606.
[63] U. Brossmann, R. Wurschum, U. Sodervall, H.E. Schaefer, Oxygen diffusion in ultrafine grained monoclinic ZrO_2, J. Appl. Phys. 85 (1999) 7646–7654.
[64] C.H. Ko, K. Kerman, S. Ramanathan, Ultra-thin film solid oxide fuel cells utilizing un-doped nanostructured zirconia electrolytes, J. Power Sources 213 (2012) 343–349.
[65] A.K.N. Kumar, S. Prasanna, B. Subramanian, S. Jayakumar, G.M. Rao, A transmission electron microscopy and X-ray photoelectron spectroscopy study of annealing induced gamma-phase nucleation, clustering, and interfacial dynamics in reactively sputtered amorphous alumina thin films, J. Appl. Phys. 117 (2015) 125307.